Chapter 2

A deterministic model of the temporal variation of the geomagnetic field

The art of prophecy is very difficult –
especially with respect to the future.
Mark Twain

Much of the scientific controversy regarding the origin of geomagnetic jerks is certainly a result of the difficulty in distinguishing between fields of external and internal origin. It is also very puzzling, that the appearance of jerks and solar maxima in the last three decades coincide suggesting a coherent cause. However, the most clearly observed jerk, which occured around 1969, appeared in period where the solar maximum was weaker than the adjacent ones, and the jerks around 1958 and 1978 were not observed globally (c.f figure 2.1 and 2.2).

This chapter presents an attempt to describe the geomagnetic field variation in terms of a deterministic model. For this study the magnetic field measurements of three observatories are examined. The first step is to look at a variety of measures of magnetic activity to explore the periodicity which one might expect in geomagnetic field measurements. I seek to eliminate the variations caused by external field fluctuations from a time series of geomagnetic observations in three Magnetic observatories Eskdalemuir (ESK, Scotland) Hermanus (HER, South Africa) and Kakioka (KAK, Japan) to gain some insights onto the short term variations caused by internal processes. The procedure relies on a deterministic model of these fluctuations and the steady secular variation. Therefore geomagnetic records of the period 1957 – 2001 are examined; while this extends outside our main period of interest, the most studied and strongest geomagnetic jerk appeared in this period, around 1969.

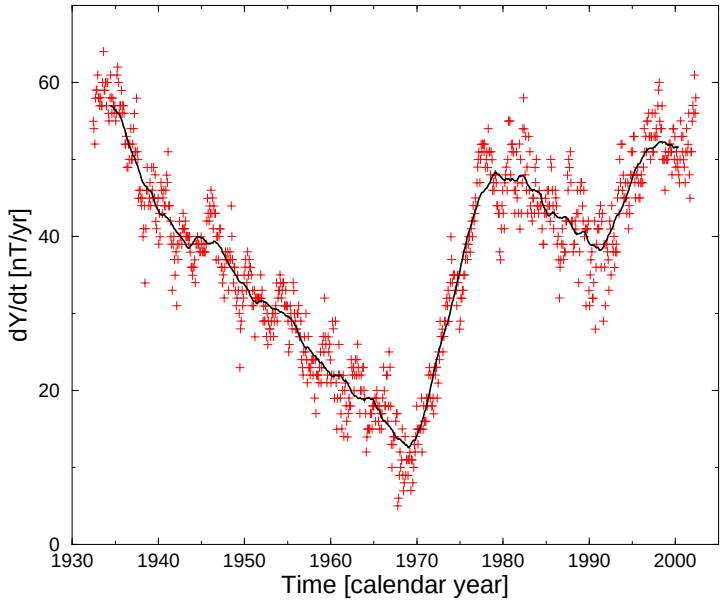

Figure 2.1: The secular variation of the east magnetic component (dY/dt) for Eskdalemuir (Scotland) from 1932 to 2002 (red dots). The black solid line is a moving average of the red dots. The geomagnetic jerks, around 1969 and 1991 are both present in the series. The jerk around 1999 is less clear.

2.1 Analysis of the external field variation

The interactions of the solar wind with the Earth's core field, influencing the dynamics of the magnetosphere and ionosphere, cause secondary magnetic fields (external fields) [Chapman & Bartels, 1940] and the fluctuation of these external fields induces currents in the lithosphere which result in tertiary time varying fields (induced fields) [Banks, 1969]. These field contributions are subsumed as disturbance fields and are directly linked to solar activity. As good proxies for solar–related disturbances the sun spot numbers, the EUV–Index, Ap–Index and D_{ST}–Index are analyzed to reveal typical time scales for disturbance field contributions.

The sun spot numbers (SSN) are defined as

$$N_Z = k(10g + n),$$

where k is a correction factor for the observer, g the number of identified sun spot groups and n the number of individual spots. These numbers, also known as Zürich numbers, were introduced by Wolf in 1848 and provide the longest continuous measure of solar activity. They show a quasi periodic variation of 10.6 years, which is referred as solar cycle. The SSN directly indicate the solar activity: high SSN connote high solar activity.
The EUV–Index represents the extreme ultraviolet flux, produced by the sun, integrated from 1 – 105 nm. Its units are $\mathrm{Wm}^2\ \mathrm{H}^{-1}$.
The Ap–Index monitors the disturbances in the horizontal field components caused by

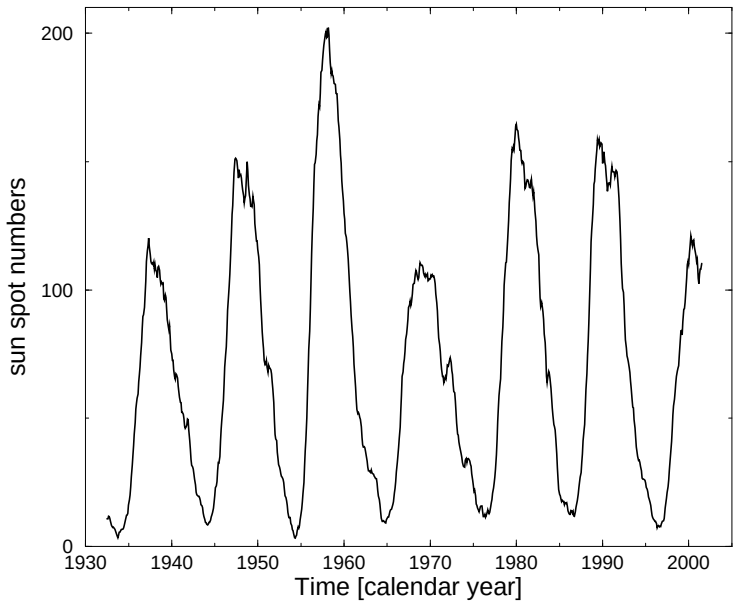

Figure 2.2: Smoothed and monthly averaged sun spot numbers, from 1932 to 2002.

solar particle radiation. It is calculated from 13 geomagnetic observatories, and reflects disturbances of the Earth's magnetic field due to solar activity.
The D_{ST} (Disturbance storm-time) index represents the axially symmetric disturbance of the magnetic field at the dipole equator on the Earth's surface [Sugiura, 1964]. D_{ST} values above -20 nT correspond to quiet behaviour of the field, values below -50 nT indicate a moderate disturbance in the field. In extreme cases, D_{ST} can drop to below -400 nT. D_{ST} is measured by a equatorial chain of observatories, which send their data to the World Data Centre for Geomagnetism, Kyoto[1]. Because preparing the D_{ST}–index for scientific study is a complex process, several versions of D_{ST} are released, from quick-look D_{ST} which is released between 12 and 36 hours after the measurements are made, to the definitive D_{ST}–index, which arrives several years afterwards.
In order to quantify typical frequencies of the disturbances and the magnetic activity external to the Earth the spectral power density function (SDF) of the SSN, EUV–, Ap– and D_{ST}–Index are estimated, from data covering the period form 1932 – 2001, and also for the, where data are available from 1957 – 2001.

A variety of spectral analysis techniques have been widely employed in the analysis of geophysical processes [Brillinger, 1981, and references therein]. More sophisticated methods have been developed which make more realistic assumptions to the irregular oscillatory behavior (noise) expected in these signals. Among these techniques, the multi–taper method (MTM) for estimations of the SDF is one of the most promising [Park et al., 1987a,b; Ghil et al., 2002].

[1](http://swdcdb.kugi.kyoto-u.ac.jp/)

2.1.1 The multi–taper method

The multi–taper method (MTM) makes use of a multiple orthogonal data taper to describe structures in time series that are modulated in frequency and amplitude. This method provides a spectral estimate with an optimal trade–off between spectral resolution and variance.

Conversely, the standard approach has been to multiply a time series by a data taper (data window such as Hanning, Blackman, Parzen, etc.) which arises when performing a discrete Fourier transform (DFT) to reduce the spectral leakage [see Percival & Walden, 1993, for details on tapering]. The use of only a single taper leads to large variances of the estimates of the SDF. Thomson [1982] introduced the use of multiple orthogonal tapers to avoid this problem and to minimize the spectral leakage. The optimal tapers are defined as the eigenvectors of a minimization problem [Slepian, 1978; Thomson, 1982].

For a given time series F(t), a set of k orthogonal tapers $a_k(t)$ and their Fourier transforms are determined

$$Y_k(f) = \sum_{t=1}^{N} a_k(t) F(t) e^{i2\pi f t \Delta t}\,, \tag{2.1}$$

where N is the number of data, f the Fourier frequency and Δt the sampling interval. From (2.1) the multi–taper power spectrum is constructed as

$$S(f) = \frac{\sum_{k=1}^{K} \lambda_k |Y_k(f)|^2}{\sum_{k=1}^{K} \lambda_k}\,. \tag{2.2}$$

λ_k measures the fractional leakage associated with the k^{th} data taper [see Percival & Walden, 1993, for the choice of the λ_k].

2.1.2 Statistical confidence

Discriminating statistics are essential in geophysical studies, where the nature of the temporal variation is complex. A pure line test as given by Mann & Lees [1996] to verify the significance of spectral features against the null hypothesis of a red noise background is utilized here. The red noise hypothesis is a reasonable description of the slowly varying geomagnetic continuum, i.e., secular variation. Significance levels are computed from the quantiles of a chi–squared distribution, assuming that the spectrum has degrees of freedom $\nu \approx 2k$. For our analysis we disregard spectral features below 99% significance.

2.1.3 Results

The spectra of the sun spot numbers and the activity indices show a complex structure, this will not be discussed in detail here. Only those periodicities and harmonics are emphasized which have significant power. At the very low frequency range, at 0.04 cycles/year the 22 years period of the solar turnover is appearing, but the dominating signal in all spectra is the solar cycle at the low frequency end of the spectrum, figure 2.3 (left). The harmonics

of this signal, 0.185 and 0.41 cycles/year (5.4 and 2.45 years period) are also resolved in this spectrum. The peak around 0.71 cycles/year (1.4 years) has been already reported [e.g., Fraser-Smith, 1972; Delouis & Mayaud, 1975; Gonzalez & Gonzalez, 1987] and shows close relation to the sector structure variation of the interplanetary field as well as the occurrences of auroras [Silverman & Shapiro, 1983] and the solar wind speed variation [Paularena et al., 1995; Krivova & Solanki, 2002].

In the intermediate and short-period branch of the spectrum of the sun spot numbers, four peaks are most clearly detectable: 2.35 cycles/year (155 days), 3.76 cycles/year (97 days), 13.5 cycles/year (27 days), 27 cycles/year (13.5 days) and 40.5 cycles/year (9 days). The first variation is related to the recurrence of the solar flares. The solar rotation period shows up as a hump at 13.5 cycles/year; its broad appearance is due to the different rotation period of sun spots at different solar latitudes. Spots close to the solar equator rotate faster than the ones towards the poles. During each solar cycle the spot locations move from $\pm$ 35° latitude towards the equator. The peak at about 27 cycles/year, half the solar rotation, originates from two high speed streams per solar rotation. According to the tilted solar dipole model, such two-stream structure appears if the heliospheric current sheet is narrow and tilted [Mursula & Zieger, 1996].

All of these periodicities are apparent in the EUV–Index and also in the spectra of the proxies of geomagnetic activity and disturbance field, see figures 2.4, 2.5 and 2.6. Further, the geomagnetic activity indices feature three additional periods. An annual fluctuation appears due to variation of the solar wind speed. It is known [Zieger & Mursula, 1998], that the solar wind speed is asymmetric with respect to the solar equator. And as the Earth revolves around the sun it changes its heliocentric latitude from 7.2° to −7.2°; thus, it is affected by different solar wind conditions in its equinoxes. A semi–annual line is also evident in the spectra of geomagnetic activity indices, most likely caused by geometrical variation of the ring current, a current system in the sunlit magnetosphere at 5 - 6 Earth's radii distance. Furthermore a period of 9 days is clearly visible in the spectra of Ap – and D_{ST}–index, which is believed to be the second harmonic of the solar rotation. Table 2.1 lists all significant signals, their frequency, periods and origin.

2.2 The formalism for the deterministic modelling of the disturbance fields

In this section a deterministic time series model is developed to eliminate the variation of the disturbance fields and the long term behaviour of the secular variation from geomagnetic field observations. This model is based on the results of the previous section and should only model these contribution for a period from 1957 – 2001.

In general the disturbances vary in a transient and irregular manner and the predominant duration of these is of the order of seconds to hours. However, a simple time averaging of the field cannot be expected to remove the effect of disturbance phenomena [Stewart & Whaler, 1992], because of the modulation by the solar cycle or longer cycles. The time

Frequency [cycles/year]	Period	Origin
40.5	9 days	possible harmonic of the solar rotation
27.0	13.5 days	two high speed streams per solar rotation
13.5	27 days	solar rotation
3.76	97 days	solar origin, but unknown cause
2.35	155 days	solar flare period
2.0	183 days	semi–annual variation
1.0	365 days	period of the Earth's revolution
0.41	2.4 yrs/894 days	solar cycle harmonic
0.18	5.4 yrs/1972 days	solar cycle harmonic
0.09	11 yrs/3872 days	solar cycle
0.04	22 yrs/7743 days	solar magnetic field turnover

Table 2.1: Periods of solar and geomagnetic activity.

series analysis of the magnetic activity indices, EUV-Index and SSN reveals at least 11 substantial periodicities, all listed in table 2.1.

2.2.1 Method

To build the deterministic model I adopt an approach introduced by Gavoret et al. [1986] and developed by Stewart & Whaler [1992] to separate external and internal signals from the geomagnetic field. The model is set up to reproduce secular variation estimates (first time derivatives) of geomagnetic field components. These are computed using, e.g.

$$X(t) = X(t + 183[days]) - X(t - 182[days])\,, \tag{2.3}$$

where t is an integer and indicates the day of the year and 182 and 183 days are the nearest integer values of half a year, respectively. The model is linearly constrained by the solar sun spot numbers (D_{ST}– and Ap–Index might be affected by secular variation, and therefore are only optionally considered in the modelling scheme) and as linear combination of sines and cosines with the typical periodicities

$$\begin{aligned} M(t) = {} & \beta_0 + \beta_1\, SSN(t) + \beta_2\, AP(t) + \beta_3\, D_{\mathrm{ST}}(t) \\ & + \sum_i [\beta_i \sin(t/T_i) + \beta_{i+1} \cos(t/T_i)]\,, \end{aligned} \tag{2.4}$$

where $M(t)$ is the prediction of the secular variation of a field component at a certain time t. The coefficients α_i and β_i are assumed to be time invariant.

$$\{T_i\} = \{9, 13.5, 27, 97, 155, 183, 365, 894, 1972, 3872, 7743\}$$

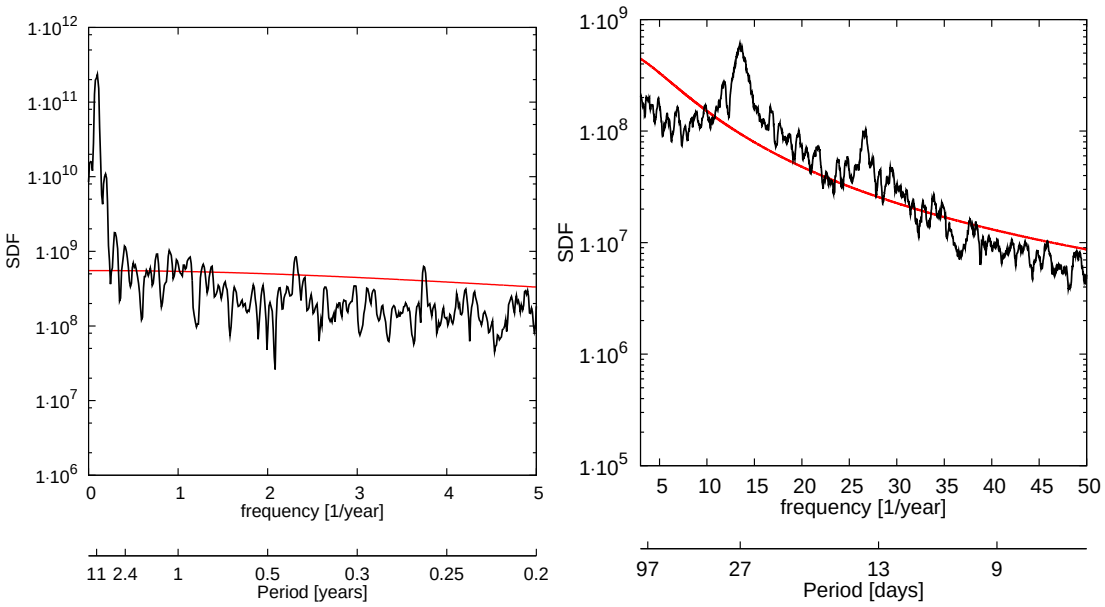

Figure 2.3: Spectral power density of the daily sun spot numbers from 1932 – 2001. The black curve is the smoothed spectrum, and the red line indicate the 90% significance level.

is the set of typical periods given in days. For the modelling, the general form of this kind of parametric model is

$$y(t) = \sum_{k=1}^{M} \alpha_k f_k(t) \tag{2.5}$$

where $f_k(t)$ are functions of t, called the basis functions and could in general be non–linear. Now defining the misfit between data and model

$$\chi^2 = \sum_{i=1}^{N} \left(\frac{y_i - \sum_{k=1}^{M} \alpha_k F_k(x_i)}{\sigma_i} \right)^2 \tag{2.6}$$

where σ_i is the measurement error of y_i (if it is unknown, it is set to $\sigma_i = 1$).
For convenience (2.5) is given in its matrix form

$$\mathsf{b} = \mathbf{A}\mathsf{x}\,, \tag{2.7}$$

where

$$\mathsf{b} = \frac{y_i}{\sigma_i}\,, \quad \mathbf{A}_{ij} = \frac{F_j(f_i)}{\sigma_i}\,, \quad \mathsf{x} = \{\alpha_1, \ldots, \alpha_k\}\,. \tag{2.8}$$

To solve this linear least–squares problem, I apply a technique known as singular value decomposition, or SVD [Golub & van Loan, 1989; Press et al., 1993]. The singular value

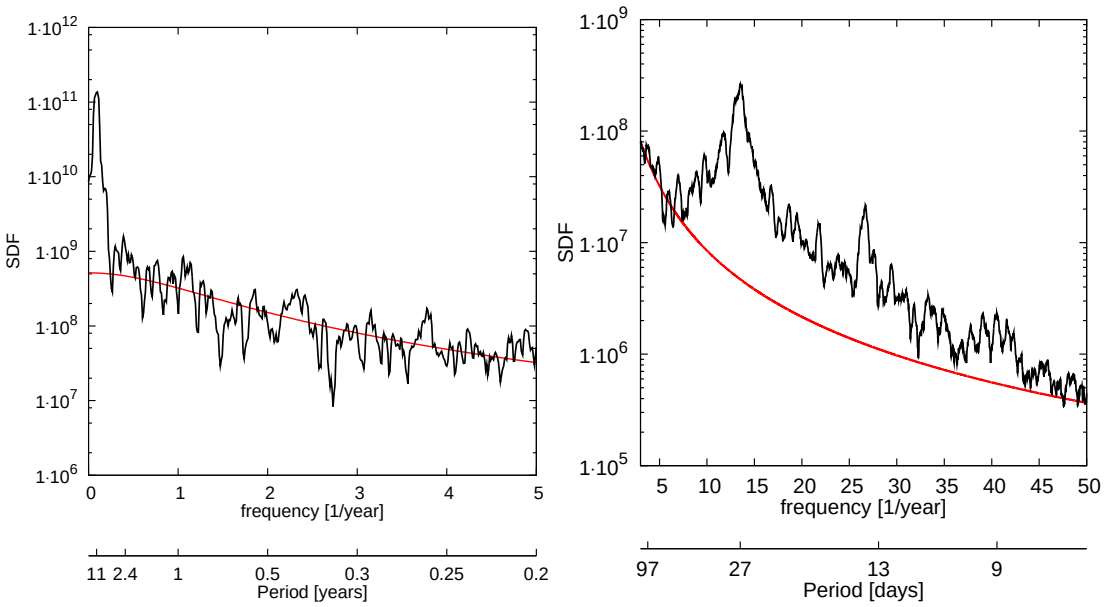

Figure 2.4: Spectral power density of the daily means of the EUV-Index from 1947 – 2001. The black curve is the smoothed spectrum, and the red line indicate the 90% significance level.

decomposition theorem says that any $M \times N$ matrix $\mathbf{A}$ whose number of rows M is greater or equal to its number of columns N has a factorization of the form

$$\mathbf{A} = \mathbf{U}\mathbf{W}\mathbf{V}^{\mathsf{T}}\,, \tag{2.9}$$

where $\mathbf{U}$ is an $M \times M$ unitary matrix and $\mathbf{V}$ is an $N \times N$ unitary matrix, both of which have orthogonal columns so that

$$\mathbf{U}^{\mathsf{T}}\mathbf{U} = \mathbf{V}^{\mathsf{T}}\mathbf{V} = 1\,. \tag{2.10}$$

$\mathbf{W}$ is an $M \times N$ diagonal matrix, whose diagonal entries are non–negative real numbers in descending order. Then the SVD provides a numerically robust solution to the least squares problem even if $\mathbf{A}$ is singular or close to singular. The general solution

$$\mathsf{x} = (\mathbf{A}^{\mathsf{T}}\mathbf{A})^{-1}\,\mathbf{A}^{\mathsf{T}}b \tag{2.11}$$

of the least squares problem becomes with (2.9)

$$\mathsf{x} = \mathbf{V}\mathbf{W}^{-1}\mathbf{U}^{\mathsf{T}}b\,, \tag{2.12}$$

where x minimizes (2.6).
The algorithm is arranged in 7 steps:

1. Find the eigenvalues λ_i of the matrix $\mathbf{A}^{\mathsf{T}}\mathbf{A}$ and arrange them in descending order.

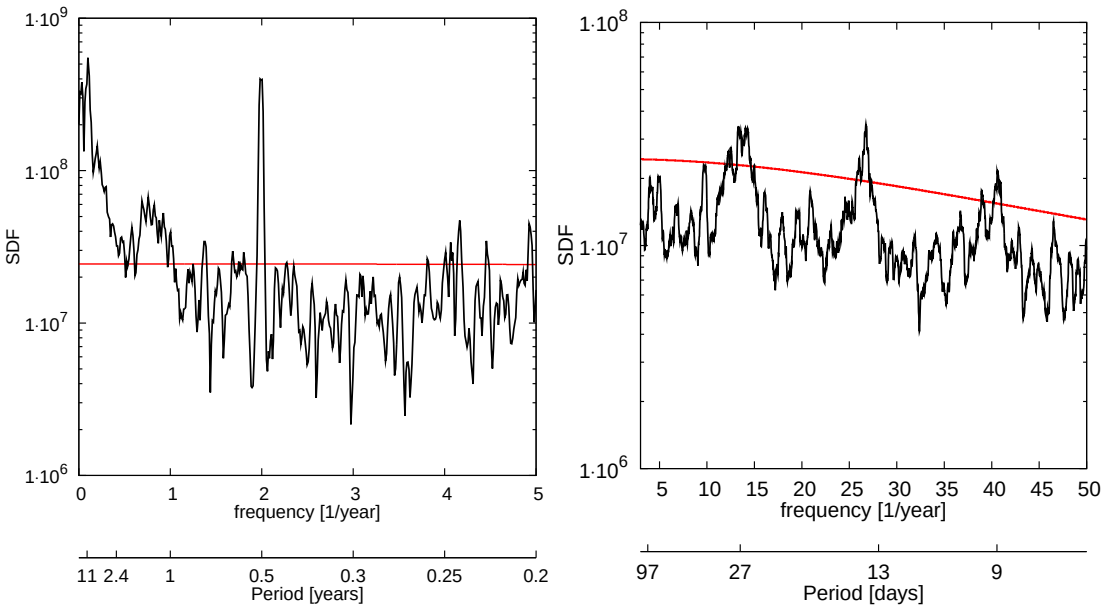

Figure 2.5: Spectral power density of the daily means of the Ap-Index from 1932 – 2001. The black curve is the smoothed spectrum, and the red line indicate the 90% significance level.

2. Find the number of nonzero eigenvalues r of the matrix $\mathbf{A}^{\mathsf{T}}\mathbf{A}$.

3. Find the orthogonal eigenvectors of the matrix $\mathbf{A}^{\mathsf{T}}\mathbf{A}$ corresponding to the obtained eigenvalues, and arrange them in the same order to form the column-vectors of the matrix $\mathbf{V}$.

4. Form a diagonal matrix $\mathbf{W}$ placing on the leading diagonal of it the square roots of first eigenvalues of the matrix $\mathbf{A}^{\mathsf{T}}\mathbf{A}$ in descending order.

5. Find the first column-vectors of the matrix $\mathbf{U}$

$$\mathsf{u}_i = (\lambda_i)^{-1/2}\mathbf{A}\mathsf{v}_i\,, \quad i = 1, \ldots, r.$$

6. Add to the matrix U the rest of m-r vectors using the Gram-Schmidt orthogonalization process.

7. Forward computation from the solution x

$$X(t)^{\text{model}} = \mathbf{A}\mathsf{x}\,.$$

Then the residuals are given by

$$R(t) = X(t)^{\text{observation}} - X(t)^{\text{model}} \tag{2.13}$$

which are expected to be the remaining internal signal.

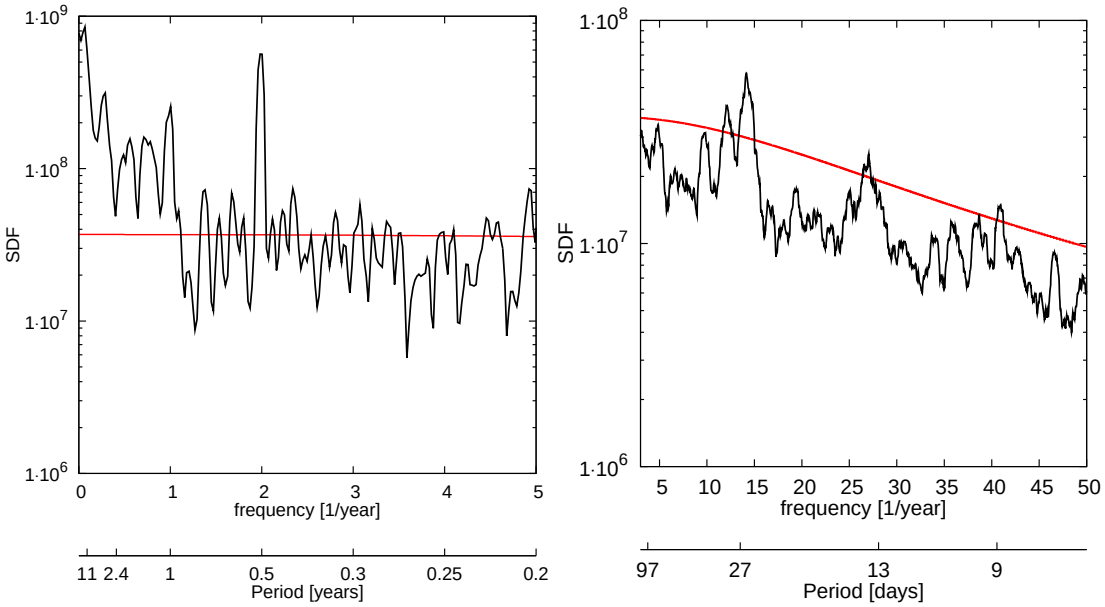

Figure 2.6: Spectral power density of the daily means of the D_{ST}-Index from 1957 – 2001. The black curve is the smoothed spectrum, and the red line indicate the 90% significance level.

2.2.2 Results and Discussion

The left panels of Fig.(2.7), (2.8) and (2.9) show the secular variation estimates of the model (red curve) and derived from the X, Y and Z components of three different observatories (black curve). The model fits the secular variation very well and even recovers the geomagnetic jerks occurred in this period, 1969 and 1991 easily seen in dY/dt at Eskdalemuir. Invoking the D_{ST}–Index reduces the residuals further, shown in Fig.(2.7), (2.8) and (2.9) (right column).

One key to interpret these results is given with the power spectra of the coefficients β_i Fig.(2.10). It shows how much of the power is accounted for the principal frequencies $\{T_i\} = \{9, 13.5, 27, 97, 155, 183, 365, 894, 1972, 3872, 7743\}$ (days) to fit the secular variation. The first 15 coefficients represent periodicities up to 365 days. These are more or less of the same order. The 16. and 17. coefficients represent the 11–year solar cycle, 18 and 19 are the coefficients for 894–days period, coefficients 20 – 23 are the ones of the 1972 and 7743 days periods and coefficients 24, 25 belong to the $SSN(t)$ and $AP(t)$. The D_{ST}-Index is not considered in this analysis. Much power is accounted to the long term variation.

In contrast, results by Yukutake [1965], who analysed the solar cycle effect to the secular variation on the basis of a spherical harmonic decomposition, indicated that this effect is rather weak. However, disregarding long term periods ($T_i > 365$ days) leaves a significant amount of unmodeled signal, as shown in Fig.(2.11), (2.12) and (2.13). In order to eval-

uate the long term behaviour a model was derived where the four longest periods $\{T_i\} = \{894, 1972, 3872, 7743\}$ were replaced by fake periods $\{T_i^f\} = \{1200, 2500, 3000, 10950\}$ (days). Table (2.2) gives the rms misfit of the three models (invoking all periods resulting from the time series analysis of solar and geomagnetic activity, the short term periods and fake periods). The rms misfits of the fake model and those of the model with the real periodicities do not differ significantly and even for Hermanus the fit is improved. Therefore, it is not clear, if the long term behaviour of the secular variation are really caused by long term external variations, such as the solar magnetic field turnover.

2.3 Arguments against the external field variations cause of jerks

I would like to argue for a non-external origin of geomagnetic jerks on ground of two arguments:

1. The effect of solar activity phenoma, such as solar magnetic field turnover, the 11 year solar cycle and its harmonics should average out and should be zonal in the Earth coordinate frame, whereas the geomagnetic jerks are not zonal by nature [see figures 17 and 18 of Alexandrescu et al., 1996].

2. Only the geomagnetic jerks occurred 1969, 1991 and clearly detectable in the Y component of European observatories, show a conspicuous 22–year period, but why are there no jerks around 1947 detectable in Eskdalemuir?

This line of arguments does not rule out a linkage of the solar magnetic field turnovers and the occurring of geomagnetic jerks, but the evidence is rather weak. As these models are only valid for a single location a much stronger persuasiveness would have the results of the same analysis, but carried out on a time–dependent model of the internal field, i.e. *GUFM*. A future plan could be the description of the Gauss coefficients belonging to such model by a single deterministic model.

Observatory	Model	X	Y	Z
Eskdalemuir (ESK)	all	12.7953	8.86353	14.4843
	short term	16.3296	14.8127	16.7678
	fake	12.9739	9.10849	16.5145
Kakioka (KAK)	all	21.4368	5.29365	10.10121
	short term	24.7739	8.35060	24.5176
	fake	21.5067	5.67791	10.7869
Hermanus (HER)	all	20.8919	8.80827	9.64212
	short term	28.3469	18.0062	10.9068
	fake	20.9287	8.57450	9.62499

Table 2.2: The rms misfit for three different observatories and three deterministic models.

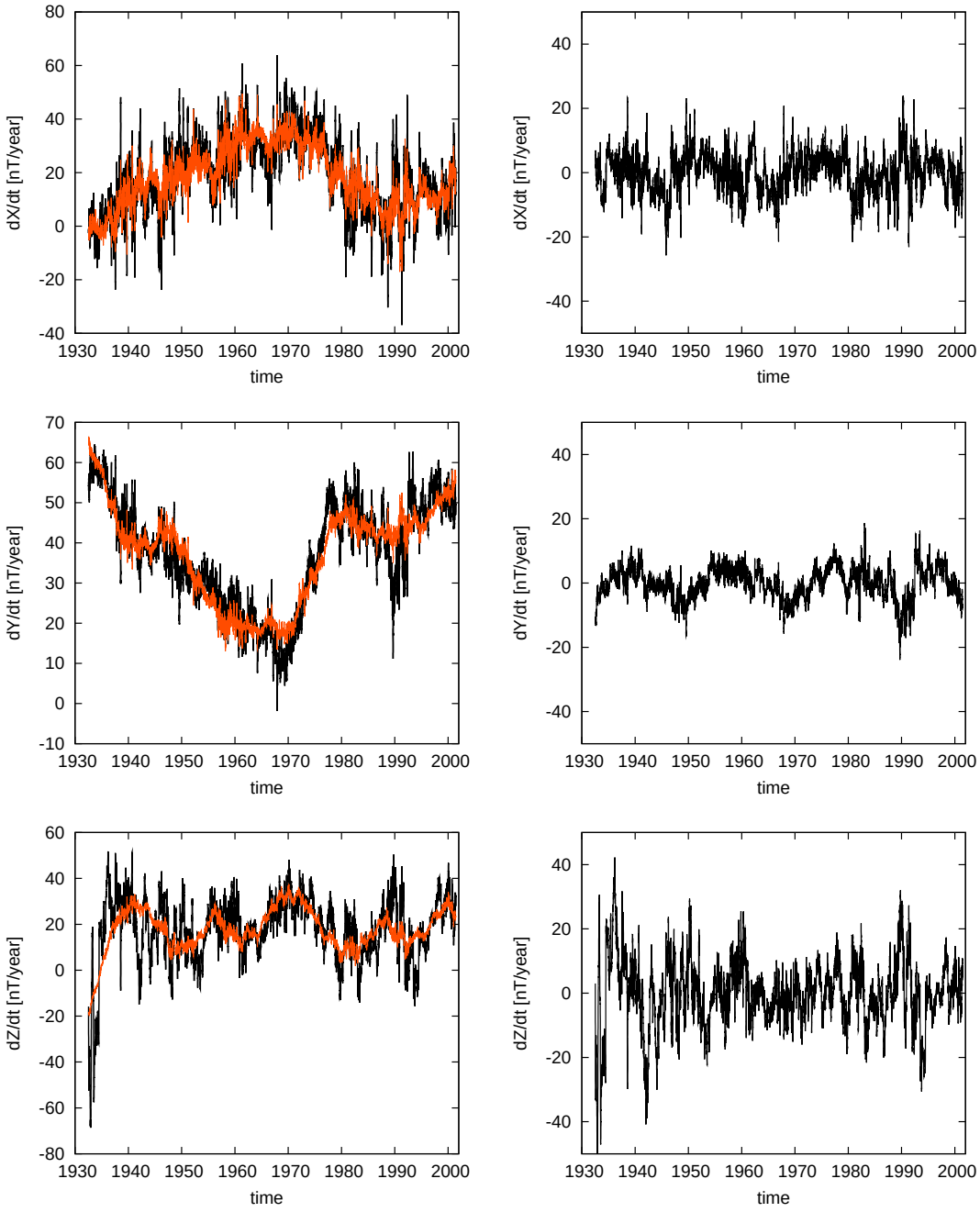

Figure 2.7: The left figures are the direct comparison of the prediction of deterministic model (red curve) valid for the period 1932 – 2001 and secular variation estimates for the X, Y and Z component in Eskdalemuir (from top to bottom, black curves). All curves are smoothed by a moving average of 20 days. The right column pictures are the remaining signal, the residuals, which cannot be explained by the deterministic model (red curve). The black curve represents the smoothed residuals.

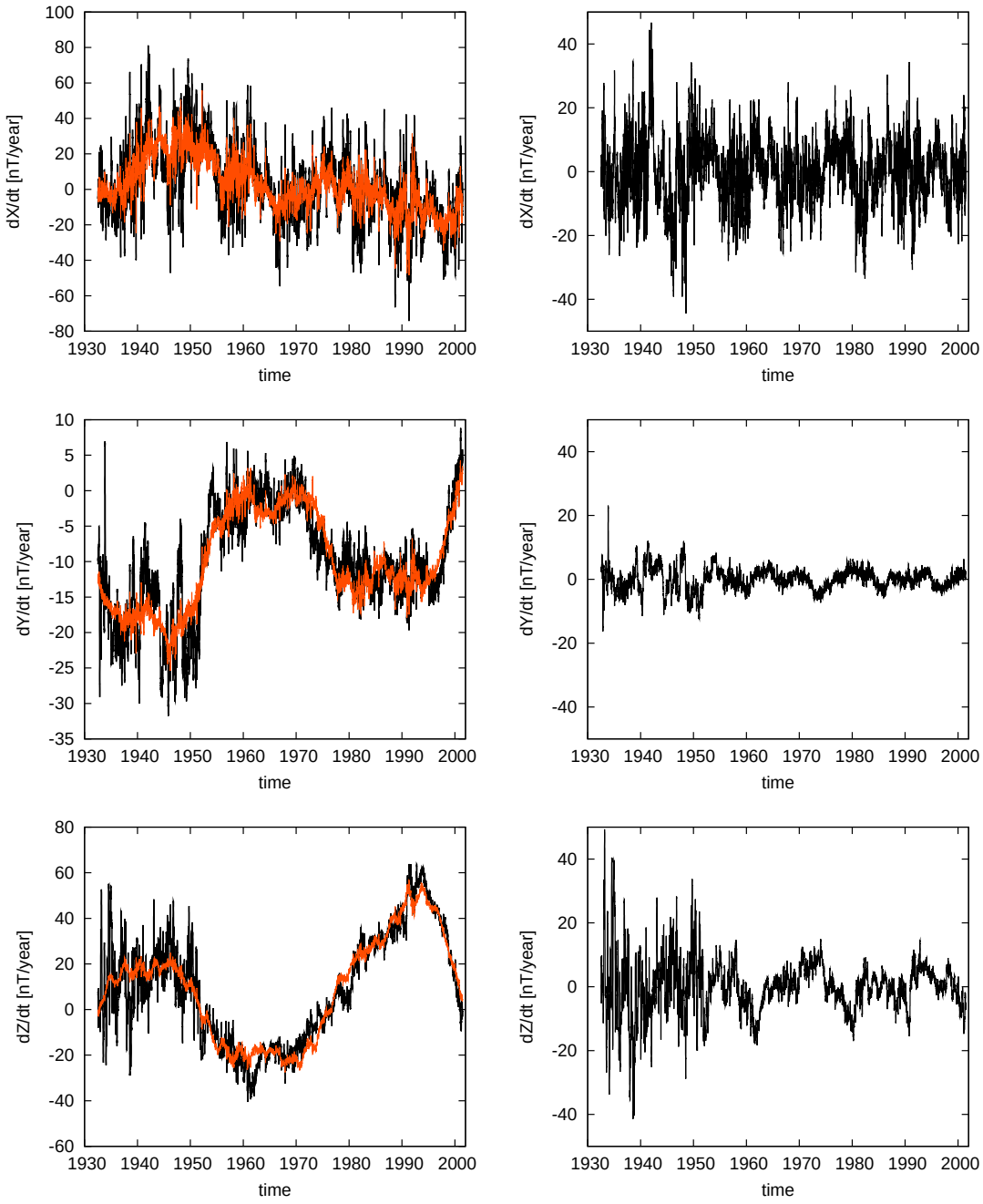

Figure 2.8: The fit to the secular variation estimates for the X, Y and Z component in Kakioka. Curves are assembled and smoothed in same way as in Fig.(2.7).

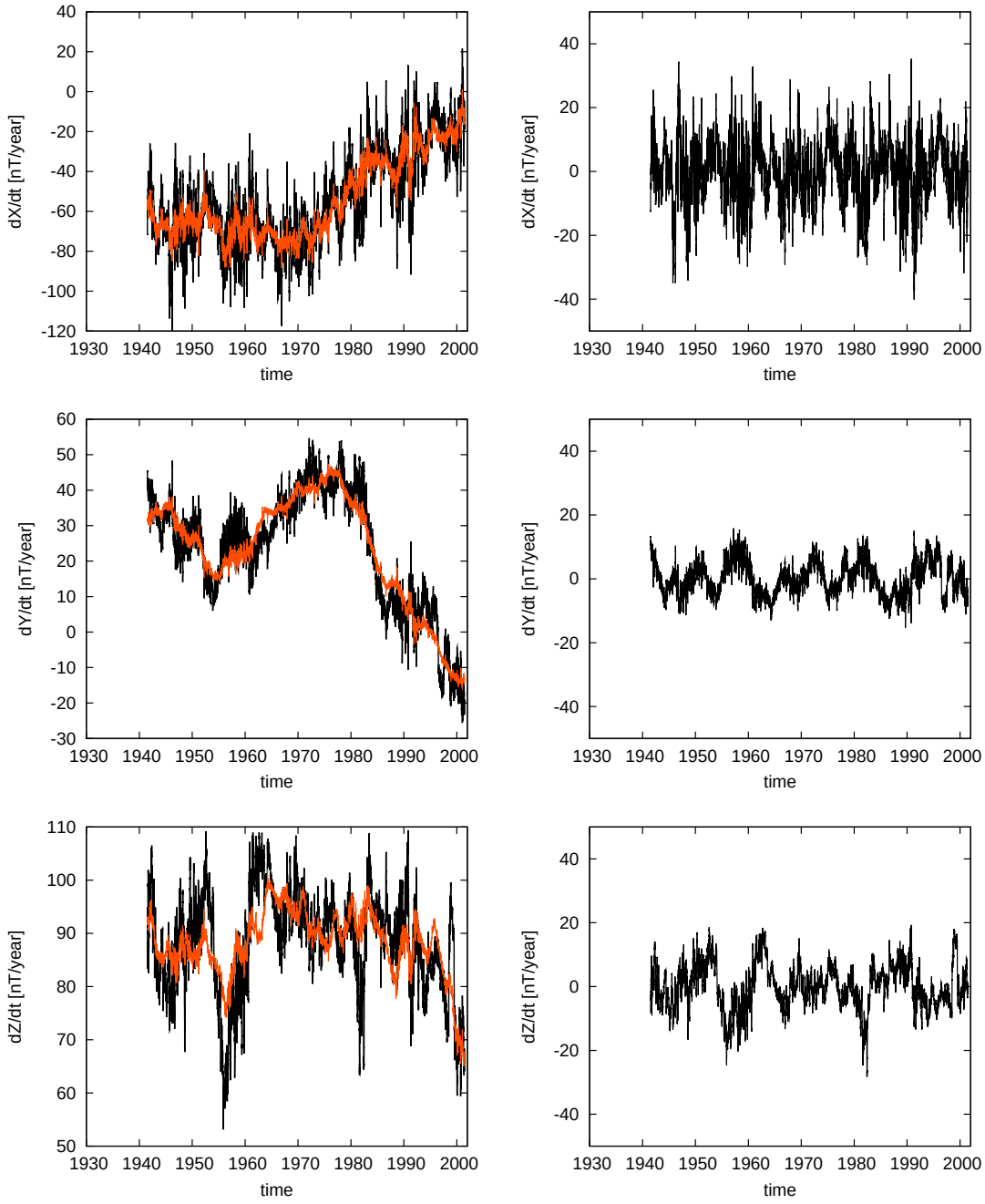

Figure 2.9: Shown here the fit for the secular variation estimates for the X, Y and Z component in Hermanus for the period 1941 – 2001. Curves are assembled and smoothed in same way as in Fig.(2.7).

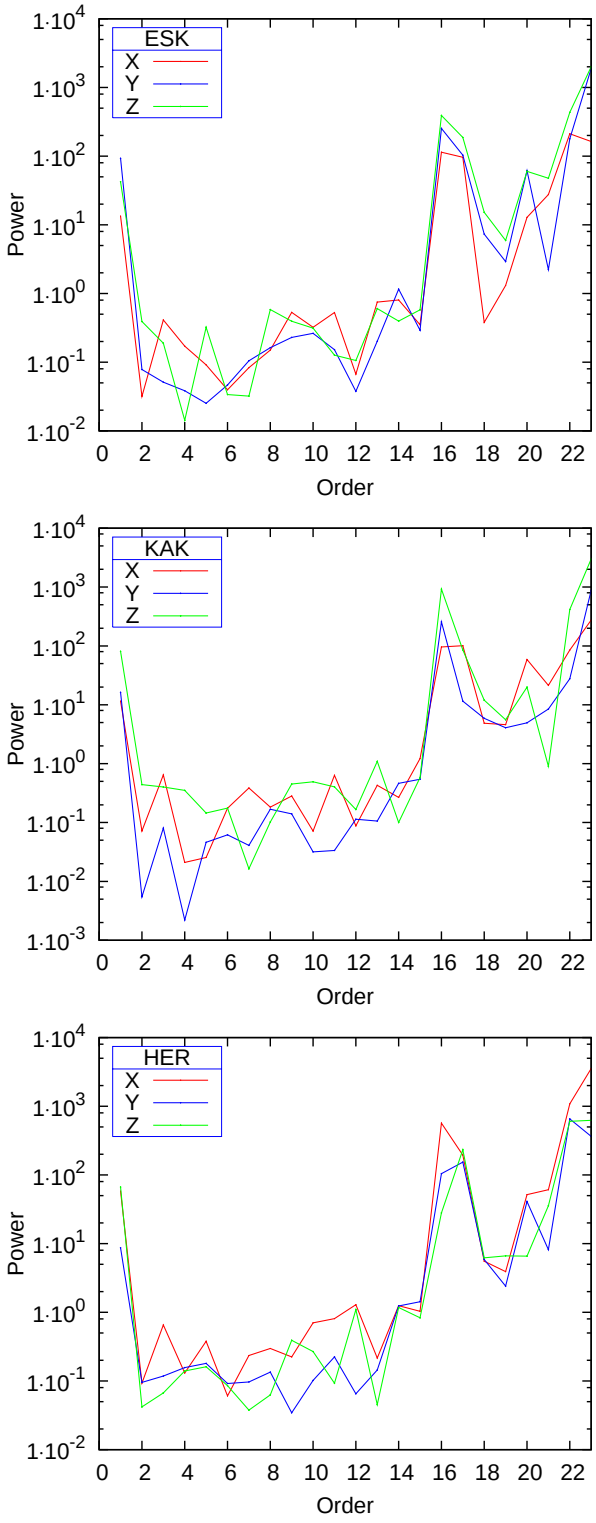

Figure 2.10: Spectra of the principal components coefficients for X, Y and Z of the analysis of the three sites Eskdalemuir (ESK), Kakioka (KAK) and Hermanus (HER).

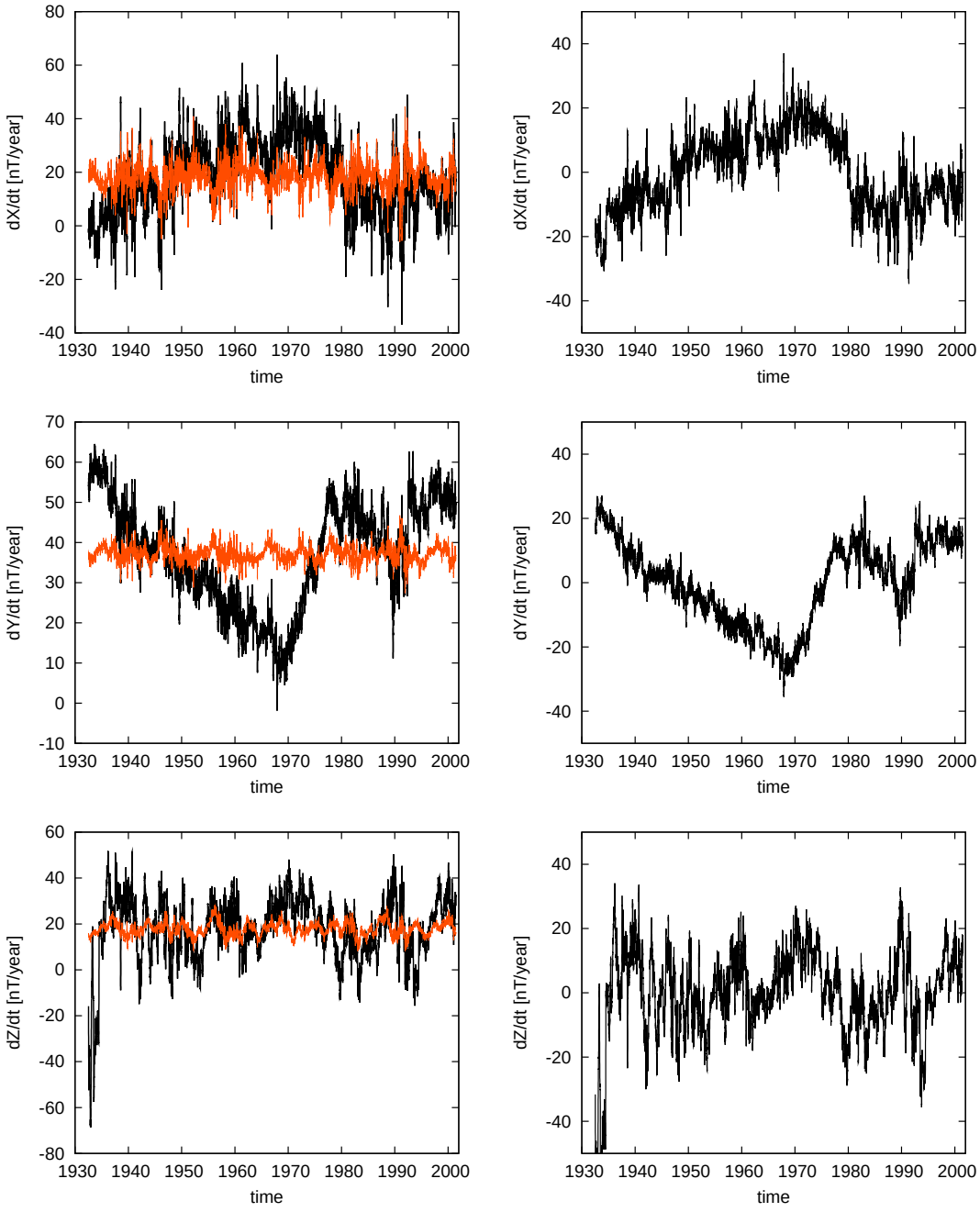

Figure 2.11: The left figures are the direct comparison of the prediction of deterministic model considering only short periods (red curve) valid for the period 1932 – 2001 and secular variation estimates for the X, Y and Z component in Eskdalemuir (from top to bottom, black curves). All curves are smoothed by a moving average of 20 days. The right column pictures are the remaining signal, the residuals, which cannot be explained by the short periods of the deterministic model (red curve). The black curve represents the smoothed residuals.

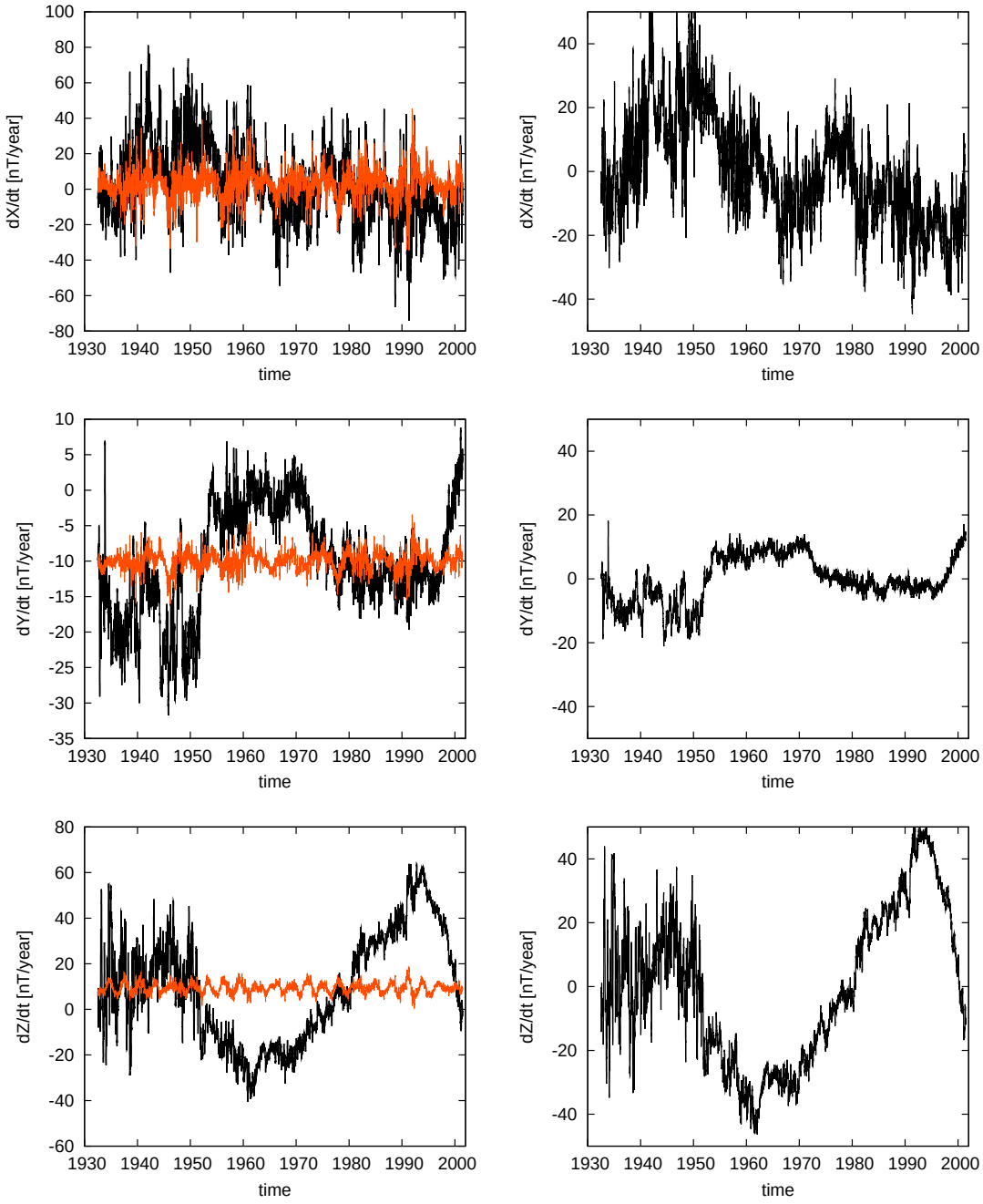

Figure 2.12: Shown here the fit for the secular variation estimates for the X, Y and Z component in Kakioka for short periods only. Curves are assembled and smoothed in same way as in Fig.(2.11).

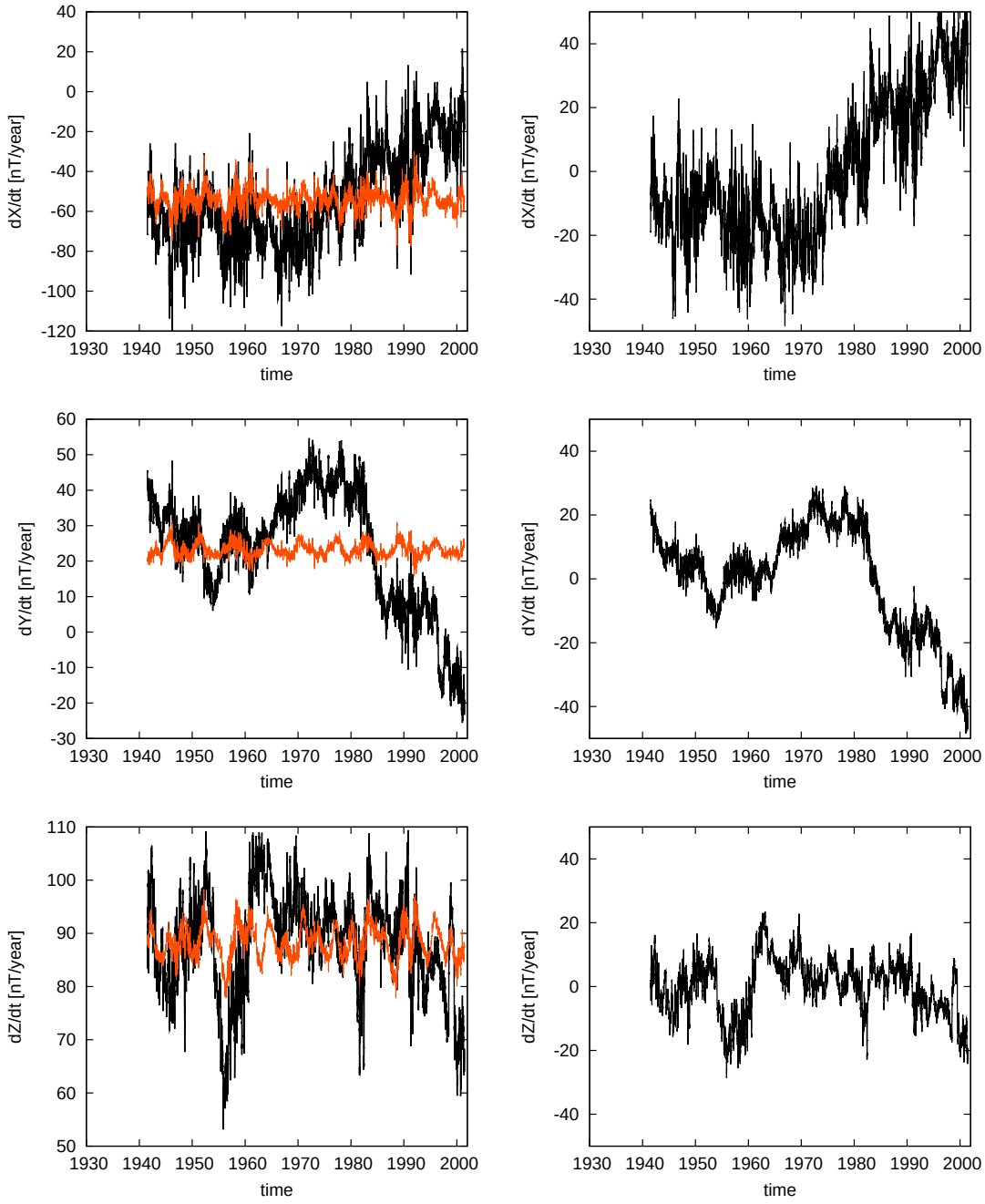

Figure 2.13: Shown here the fit for the secular variation estimates for the X, Y and Z component in Hermanus for short periods only. Curves are assembled and smoothed in same way as in Fig.(2.11).

2.4 Conclusions

In this chapter a method has been developed specifically for the analysis of the influence of solar related activity phenomena to the geomagnetic field at a individual location. The algorithm considers all significant periodicities deduced from a time series analysis of the sun spot numbers, EUV–, D_{ST}– and Ap–Index. Then the algorithm is set up to model the geomagnetic field variations as a superposition of harmonics of these periodicities. The model fit is achieved in linear least squares sense by using a singular value decomposition. Observation and predictions for each magnetic field component are differentiated in time to gain a secular variation estimate and then compared to each other. Consequently, the unmodeled signal, which cannot be explained in terms of disturbance field variation, should therefore represent the noise-free secular variation.
This analysis reveals that almost all of the secular variation can be explained by a simple deterministic model, which superpose all significant periods of solar and Earth–Sun interaction phenomena. But caution has to be paid for two reasons: First, a simple model which is partly built up with artificial long periods (fake model) explain the secular variation at the three station evenly good as the real deterministic model. Secondly, the fact that this model is not capable of distinguishing between external and internal variations on the basis of typical time scales of those variations, is important. And therefore, the conclusion drawn from the comparison of the observations between the model predictions, that the geomagnetic jerks originate externally is not necessarily correct. The rest of this thesis will consider a model of the field observations based on an internal field. With this model, I will be able to fit the jerk signal, suggesting further that jerks are primarily of internal origin.